Structural and spectral features of nano-crystalline copper-stabilized zirconia

Veda Ramaswamy, Mahesh Bhagwat, Darbha Srinivas,
Arumugamangalam V. Ramaswamy*

National Chemical Laboratory, Catalysis and Inorganic Chemistry Division, Pune 411008, India
Available online 31 July 2004

Abstract

The structural and spectral characteristics of copper-stabilized zirconia samples with different Cu contents (0.1–30 mol % of Cu), prepared by co-precipitation and sol–gel techniques are reported. The samples are designated as Cu–ZrO$_2$(n), where 'n' is the Cu content in mol %. Rietveld analysis of the powder X-ray diffraction (XRD) data reveals that copper stabilizes zirconia both in cubic and tetragonal phases in all the Cu–ZrO$_2$ compositions. With increasing concentration of Cu, zirconia is stabilized more and more in the cubic phase than in the tetragonal phase. A decrease in the crystallite size (from 28 to 8 nm) is also noted. Electron paramagnetic resonance (EPR) and diffuse reflectance UV–visible (DRUV–Vis) spectroscopies reveal that the samples contain at least four different types of paramagnetic Cu species, depending on the Cu content. These are isolated Cu^{2+} ions substituted in the framework sites of Zr^{4+} (species I), charge compensating ions located in the interstitial positions (species II), dispersed Cu ions bound to the surface (species III) and CuO-type clusters at the surface (species IV). Species I and II are present in all the Cu–ZrO$_2$ compositons. Species III is present only in the samples containing more than 5 mol % Cu in zirconia. Species IV is found in the samples with still higher Cu content ($\geq$20 mol %); this species on treatment at high temperature (1173 K, for example) disintegrates yielding a separate bulk CuO phase. Species I is more difficult to reduce than species II–IV, even at 973 K using dry hydrogen. Electrons trapped in anion vacancies and O$^-$ radicals are also detected by EPR under the conditions of evacuation, pretreatment and reaction with hydrogen. The spectral studies reinforce the conclusions drawn from XRD that some amount of Cu is incorporated in the zirconia lattice. The copper ions are dispersed up to a Cu concentration of 20 mol % in zirconia. The high catalytic activity of Cu–ZrO$_2$(20) samples in CH$_4$ and CO oxidations reported earlier is attributed to the highly dispersed nature of Cu ions in zirconia, their facile redox property (Cu^{2+} to Cu$^{+1/0}$) and oxygen storage capacity of the support oxide.
© 2004 Elsevier B.V. All rights reserved.

1. Introduction

Zirconia as a material finds many applications as refractory, piezoelectric devices, ceramic condensers and oxygen sensors due to some of its unique properties such as high hardness, low wear resistance, low coefficient of friction, high elastic modulus, chemical inertness, low thermal conductivity and high melting point [1]. Zirconia is also a good catalyst support, since it is amphoteric, has a high thermal stability and can be prepared with a reasonable BET surface area. [2]. Sulfated zirconia is well known as a solid super acid that has found many interesting applications in alkylation and other acid-catalyzed reactions [3]. On the other hand, zirconia doped with other metal oxides has been investigated for redox reactions. Earlier ZrO$_2$ doped with alkaline, alkaline earth and rare earth metal oxides such as CaO, MgO, Y$_2$O$_3$, La$_2$O$_3$ and Ce$_2$O$_3$ have been studied [4–8]. These reports have essentially dealt with the phase changes of zirconia accompanied by the introduction of these oxides through solid-state transformations. Subsequently, the transition metal oxides such as CuO, Cr$_2$O$_3$, Fe$_2$O$_3$, MnO$_2$ and NiO have been incorporated into zirconia with the possible use of them as catalysts in oxidation

* Corresponding author. Present address: Department of Chemistry, University of Pune, Pune 411007 India. Tel.: +91 205893761; fax: +91 205894761.
E-mail address: avram@chem.unipune.ernet.in (A.V. Ramaswamy).

reactions. The introduction of these metal oxides has been through a number of preparation techniques, impregnation, co-precipitation, sol-gel and so on through which these multivalent metal oxides could be well dispersed on zirconia, since effective dispersion of these active metal oxides contribute to enhanced catalytic activity [9–13]. We have earlier reported on the catalytic activity of some of these materials in the oxidation of hydrocarbons and CO [11]. Among these materials, zirconia-supported copper (Cu–ZrO_2) catalysts have attracted considerable attention in recent years [14–28]. Among some of the interesting catalytic reactions that employed Cu–ZrO_2, we may mention the reports on the abatement of NO_x with propene or ammonia in presence of dioxygen [14–16,28] and methanol synthesis from CO_2 or CO and H_2 [17–21]. For the total oxidation of CO, the zirconia-supported Cu catalysts showed higher activity than the alumina-supported catalysts [9]. Morterra et al. [22] reported on the decomposition of N_2O at 723 K. These catalysts were also used for hydrogen generation by direct oxidation of hydrocarbons [23–26]. Dongare et al. [27] have found that Cu–ZrO_2 catalysts, with cubic (fluorite) structure, prepared by the sol–gel technique exhibit efficient catalytic activity in CH_4 and CO oxidation. In a series of samples with different Cu contents, Cu–ZrO_2 with 20 mol % Cu was found to be the most efficient sample.

Among the various factors, dispersion of the active phase, nuclearity, oxidation state and structural and redox properties of the supported metal ions influence the catalytic activity of the materials. With reference to the structural properties of zirconia, which alter as a function of temperature or doping of metal atoms in the lattice, there are discrepancies in the reports. There are three well-defined polymorphs of zirconia. The monoclinic phase is stable up to 1447 K. It then transforms into the tetragonal phase, which further changes into the cubic phase at 2643 K. The cubic phase is stable up to the melting point (2953 K) of zirconia. The nature of the phase governs the physical properties of zirconia and the cubic phase turns out to be very interesting from the point of view of stability of the material in applications as advanced ceramics. The main aim of using these metal oxides as dopants is to obtain zirconia in the cubic phase at lower temperatures of calcination.

Formation of the low temperature-stable or meta-stable cubic or tetragonal phase and the corresponding phase transformations as a function of temperature has been explained by various theories [29–32]. The metal ions used as dopants are generally of smaller size and lower valent (compared to Zr^{4+} ions) and if the Zr^{4+} ions in the lattice are substituted by these metal ions, one would expect a decrease in the unit cell volume and generation of positive holes with lattice defects (oxygen vacancies). It is proposed that these defects in the zirconia lattice play a major role in stabilizing the system in a cubic phase. While several studies reported the stabilization of zirconia in the cubic phase [11,27,33–35], some reports point to the formation of a pseudotetragonal phase [36,37] on metal doping. It is also reported that

low temperature tetragonal phase is formed even without the addition of any dopent [38]. We have recently shown through Rietveld refinement of powder XRD profiles that Cu-doped zirconia is stabilized in both cubic and tetragonal phases, depending upon the concentration of Cu, and the temperature of treatment [39]. These stabilized or partially stabilized zirconia phases have been used in a number of catalytic reactions, as oxygen pumps and as gas sensors where these properties of zirconia are structure-dependent. Many of the factors responsible for the catalytic activity are, in turn, dependent on the metal content, the method of preparation and pretreatment conditions. In the present report, we describe the Cu–zirconia system in detail, prepared by the sol–gel and co-precipitation techniques with different levels of Cu in zirconia. We employ mainly two techniques for the characterization of the samples. The first one is powder XRD followed by Rietveld refinement of the profiles to give information on the long-range order in the samples. Rietveld refinement has been used to overcome the problem arising from overlapping reflections of the three polymorphs. The second is the EPR technique, along with UV–Vis spectroscopy to differentiate Cu in different environments and to look at the short-range order. The spin Hamiltonian parameters and the ground state electronic configuration of Cu(II) are highly sensitive to the local geometry. The amount of Cu in the samples is varied from 0.1 to 33 mol %. The signals corresponding to different Cu species were separated by spectral deconvolution. The redox behavior of Cu is reported. An attempt is made to identify the active Cu species in CH_4 and CO oxidations. This characterization study complements the catalytic activity studies reported earlier [27].

2. Experimental

2.1. Materials and catalyst preparation

One set of Cu–ZrO_2 samples was prepared by co-precipitation technique. Aqueous solutions of zirconium oxynitrate and copper nitrate were mixed in the required proportion and stirred continuously for 1 h. Cu and Zr were co-precipitated as mixed hydroxides by adding tetramethyl ammonium hydroxide drop-wise to the above mixture and the pH was adjusted to 9. The hydroxide precipitate was filtered, washed with de-ionized water, dried at 373 K overnight and then calcined in a muffle furnace in air at 773 K for 9 h. Cu–ZrO_2 samples with 2, 5, 10 and 20 mol % Cu were prepared by this technique.

Another set of Cu–ZrO_2 samples were prepared by the sol–gel technique as reported earlier [27]. In a typical synthesis, 47 g of zirconium isopropoxide (70 wt.% solution in 1-propanol, Aldrich Co) was dissolved in 400 ml of dry isopropanol. To this, a stoichiometric amount of Cu(NO_3)$_2$ (LOBA Chemie) dissolved in 100 ml of isopropanol was added under constant stirring to obtain a clear, homogeneous

solution. Thereafter, a known quantity of water and a catalytic quantity of HCl were mixed in 100 ml of isopropanol and introduced into the above solution in order to hydrolyze the zirconium isopropoxide. The mixture obtained was stirred for another 1 h and allowed to stand for 12 h to result in a thick transparent gel, which was kept for drying at 298 K. The resulting glassy, solid was ground into a fine powder and calcined for 12 h at 723 K. Using different amounts of $Cu(NO_3)_2$, a series of $Cu–ZrO_2(n)$ samples were prepared, where 'n' refers to the Cu content in mol % of ZrO_2.

2.2. Powder XRD studies

The polycrystalline $Cu–ZrO_2$ samples were characterized on a Philips X'pert Pro X-ray diffractometer, using monochromatic Cu K_α radiation ($\lambda = 1.5406$ Å). The XRD patterns were recorded in the 2θ range of 20–80° with a step of 0.02° and at a scan rate of 1° min^{-1}. The sample was mounted on a Pt strip, which acted as the sample holder. The Rietveld refinement studies of the powder XRD profiles were performed using the DBWS program with a Cerius-2 interface.

2.3. EPR studies and sample treatments

The EPR spectra of the samples were recorded on a Bruker EMX spectrometer operating at 9.75 GHz frequency and 100 kHz field modulation. Microwave frequency was calibrated with a frequency counter fitted in the Bruker ER 041 XG-D microwave bridge. Magnetic field was calibrated using a Bruker ER 035 M NMR Gaussmeter. The samples were taken in specially designed Suprasil quartz tubes (o.d. ∼4.5 mm) and pretreated by evacuating (1 Pa) for 10 h at different temperatures (473–1073 K). The spectra were

recorded at 77 and 298 K. Measurements at 77 K were done using a quartz finger Dewar. In the reduction experiments, the pretreated samples were reacted with dry hydrogen (20 ml min^{-1}) for 4–5 h and then the spectra were recorded without exposing them to aerial oxygen. The spectra, in general, corresponded to more than one type of Cu species, depending on the Cu content. Spectral simulations were done by using the Bruker Simfonia and WINEPR software packages. It was difficult to get an exact fit of the experimental spectra, especially in the samples with higher Cu content, due to the presence of more than one paramagnetic species as well as the limitation of the program used. From the satisfactory theoretical fits, the spin Hamiltonian parameters of different species were evaluated.

2.4. DRUV–Vis studies

The DRUV–Vis spectra were recorded on a Shimadzu UV-2550 spectrophotometer equipped with an integrating sphere attachment (ISR-2200). Spectral grade $BaSO_4$ was the reference material.

3. Results and discussion

3.1. Powder XRD and Rietveld refinement

Fig. 1 shows multiple plots of the powder XRD profiles of $Cu–ZrO_2$ samples prepared by the co-precipitation method. Similar patterns for the sol–gel prepared samples were reported elsewhere [27]. The presence of cubic phase is reported in the Cu-stabilized zirconia, where the overlapping peaks of cubic and tetragonal zirconia could not be distinguished. The patterns given in Fig. 1 show cubic zirconia as the major phase with small concentrations of monoclinic
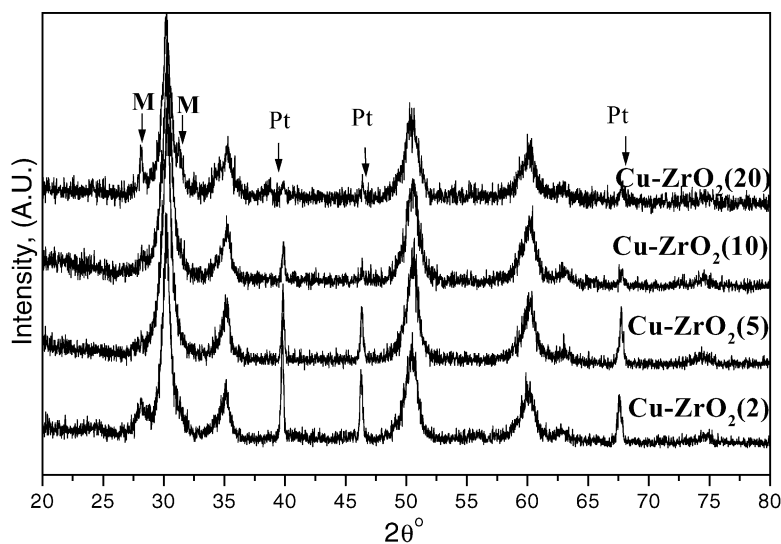

Fig. 1. Multiple plot of the powder XRD profiles of $Cu–ZrO_2(n)$ samples. Peaks denoted as Pt arise from the platinum strip used for mounting the samples and M denotes the monoclinic phase.

phase. There is a great difficulty in distinguishing between tetragonal and cubic phase because of overlapping reflections. Further, the splitting of the (040) reflection (2θ = 73.96°) of the cubic phase into (400) and (004) reflections of the tetragonal phase, which is a useful tool to distinguish between the two phases, is masked by the broad nature of the peaks, as the crystallite size is smaller. Hence, Rietveld refinement technique was used to analyze the XRD patterns. In the case of yttria-stabilized zirconia, such a refinement was reported to distinguish between the cubic phase and the metastable tetragonal phase [40]. A combination of the cubic (space group $Fm3m$), tetragonal (space group $P4_2/nmc$) and the monoclinic (space group $P2_1/c$) phases was used as the starting models for the refinement of the XRD profile of a typical sample, as neither of the combination of any two phases was successful in the refinement of the XRD pattern. The background was refined using a polynomial with six refinable coefficients. The peak shape was refined using a Pseudo-Voigt function. From the peak width, the crystallite size was calculated using the Scherer equation [41]. Various R factors obtained from the refinement results are listed in Table 1. The higher R_{EXP} (and hence, the higher R_{WP}) is due to the counting statistics being poor with the fast scan. However, the goodness of fit (G.O.F.) justifies a very good refinement of the profiles. The refinement reveals that all the Cu–ZrO$_2$ samples calcined at 773 K are not single-phase pure as both the cubic and the tetragonal phases exist and that in all the samples some monoclinic phase (Fig. 1, peaks denoted by M) remains as an impurity (about 2 wt.%). The composition of tetragonal and cubic phases varies with Cu content. As mentioned, the Rietveld refinement results indicate that zirconia is stabilized partially into tetragonal phase and partially into the cubic phase as a result of introduction of Cu into zirconia. Changes in the relative phase compositions are seen, as the concentration of Cu is increased from 2 to 20 mol % in zirconia. Table 2 presents the percent phase compositions and the changes in the unit cell volume for samples with different Cu content. It is seen that at low concentration of Cu, tetragonal phase predominates, and that there is a facile change from tetragonal to cubic phase, as the Cu content increases from 2 to 20 mol % in zirconia. The percent cubic phase increases at the expense of the tetragonal phase. The sample with 20 mol % Cu has a composition in which the cubic phase is the major component. A decrease in the unit cell volume as compared to the volume for ZrO$_2$ (V = 133.58 Å^3) with an increase in Cu concentration indicates some substitution of Cu^{2+} ions in the

Table 1
Rietveld refinement of powder XRD profiles and R factors for Cu–ZrO$_2$(n) samples

R factors	Cu–ZrO$_2$(2)	Cu–ZrO$_2$(5)	Cu–ZrO$_2$(10)	Cu–ZrO$_2$(20)
R_P	19.54	18.19	16.50	16.0
R_{WP}	27.13	25.20	23.08	21.10
R_{EXP}	23.88	22.21	21.32	19.69
G.O.F.s	1.14	1.13	1.08	1.07
D-WD	1.75	1.74	1.82	1.86

zirconia lattice. We have earlier shown that such a decrease in the unit cell volume is linear with respect to Cu content, but not proportional to the theoretical decrease of the unit cell volume based on the differences in the ionic radii of Zr^{4+} and Cu^{2+} ions [27]. It shows that only a small concentration of Cu probably gets substituted for Zr^{4+} in the lattice and that depending on the concentration of Cu, there are other locations in which Cu should exist as extra lattice copper. Another interesting observation is that the crystallite size of the cubic phase decreases from about 26 nm size for the sample with 2 mol % Cu to about 8 nm size at 20 mol % loading of Cu in zirconia (Table 2). Thus, the stabilization of zirconia in the cubic phase is related to the crystallite size of the zirconia on the one hand, and the Cu content on the other. Recently, Wang and Caruso [42] have reported the formation of tetragonal zirconia by doping with Cu using the co-precipitation technique. They reported a crystallite size of the order of 14–16 nm. Our results indicate stabilization of zirconia both in cubic and tetragonal phases with still smaller crystallite size at similar Cu loading.

3.2. EPR and DRUV–Vis studies

The nature of copper in Cu–ZrO$_2$ samples prepared by sol–gel technique is investigated by EPR and DRUV–Vis spectroscopies. Cu–ZrO$_2$ samples with less than 2 mol % of Cu showed well-resolved copper hyperfine features and narrow EPR signals (Fig. 2). The samples with higher Cu content, on the contrary, exhibited complex spectra due to overlap of signals from different types of Cu species. Spectral simulations revealed that the spectra for the samples with ≤2 mol % Cu arise from two types of Cu species I and II. Species I is characterized by a rhombic spectrum (g_x = 2.05, g_y = 2.08 and g_z = 2.35; $A_x^{Cu} = A_y^{Cu}$ = 15 G and A_z^{Cu} = 123.7 G) and species II by an isotropic spectrum (g_{av} = 2.11). The line width of species I signals is in the range of 35–50 G and that of species II is 220 G. Samples with

Table 2
Phase composition, unit cell volume and crystallite size of Cu–ZrO$_2$(n) samples

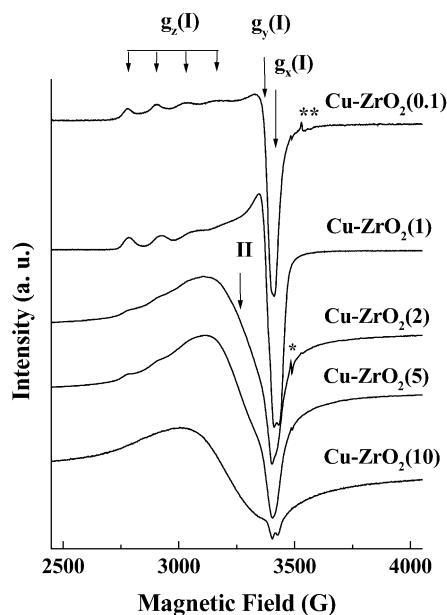| Sample	Phase composition (%)			Unit cell volume (Å^3)	Crystallite size (nm)
	Cubic	Tetragonal	Monoclinic		
Cu–ZrO$_2$(2)	31	64	5	133.46	27
Cu–ZrO$_2$(5)	36	59	5	133.02	15
Cu–ZrO$_2$(10)	45	49	6	132.70	11
Cu–ZrO$_2$(20)	51	38	11	132.36	8

Fig. 2. EPR spectra of Cu–ZrO$_2$(n) samples at 298 K. The signals due to Cu species I and II are indicated. Symbol * represents the signal due to O$^-$ ions. Symbol ** represents the signal due to electrons trapped in anion vacancies.

5 mol % and more of Cu contained a yet another species III, characterized by an axial spectrum ($g_\perp = 2.08$, $g_\parallel = 2.32$ and $A_\parallel^{Cu} = 150$ G) in addition to species I and II. Samples with still higher Cu content (≥ 20 mol % Cu) contained an additional species IV characterized by a broad signal ($g_{av} = 2.25$, line width ~ 2200 G). The simulated and deconvoluted spectra of representative samples Cu–ZrO$_2$(2) and Cu–ZrO$_2$(20) are shown in Fig. 3. Measurements at 77 K showed little effect on the EPR spectra. It was reported [14,43] that the samples prepared by impregnation and co-precipitation

methods contained only the species III and IV. The present study identifies, for the first time, species I and II in the sol–gel prepared samples. The overall EPR signal intensity increased with the Cu content up to 2 mol % and thereafter it decreased (Fig. 4). This indicates that at low concentrations, Cu ions are well separated from one another. At higher concentrations, due to spin–spin interactions, the signals broadened and the total intensity decreased. The Cu ZrO$_2$(20) sample showed a weak signal at 1600 G (Fig. 3, denoted by an asterisk) corresponding to the presence of small size Cu clusters of 2–3 atoms. In the samples with still higher amounts of Cu (≥ 20 mol %), the size of the Cu cluster is larger and could be detected by XRD as a separate CuO phase.

The DRUV–Vis spectra of Cu–ZrO$_2$ samples showed a broad d–d band at around 800 nm due to isolated Cu^{2+} ions in an octahedral environment. Intensity of this band increased with increasing Cu content. The samples with ≥ 10 mol % Cu showed two new bands at 660 and 380 nm in addition to the 800 nm band. While the band at 660 nm is due to surface-bound, dispersed Cu^{2+} having square pyramidal geometry, the latter band at 380 nm is due to 2–3-atom Cu nanoclusters.

3.3. Redox behavior of copper in Cu–ZrO$_2$

Preheating of the samples followed by evacuation has a marked effect on the total EPR signal, which decreased with an increase in the evacuation temperature. In Cu–ZrO$_2$(0.1), this decrease at 803 K is about 50% of the original total intensity. In Cu–ZrO$_2$(5), the intensity reduction was about 72%. In other words, different Cu species were affected differently by the pretreatment. The signals of species I were less affected as compared to those of species II and III in
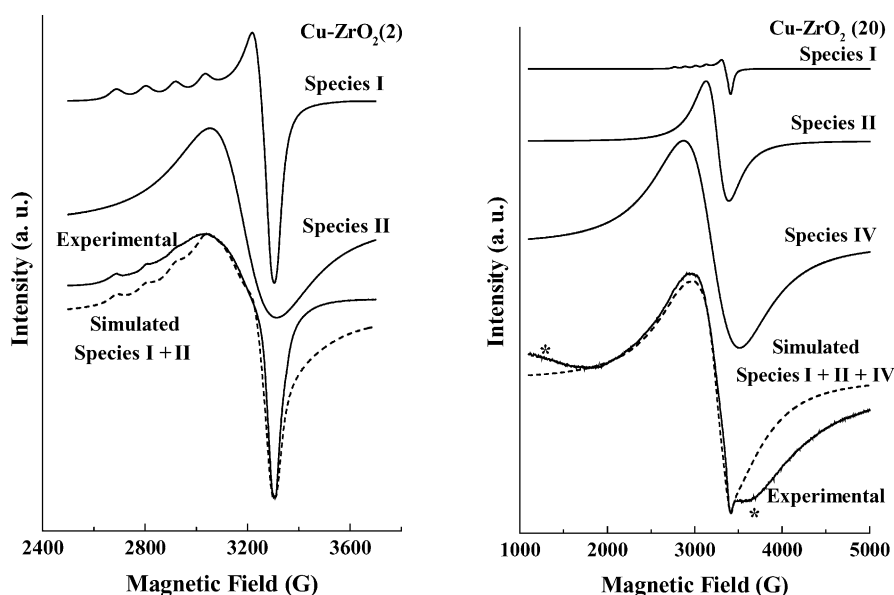

Fig. 3. Experimental, simulated and deconvoluted EPR spectra of Cu–ZrO$_2$(2) and Cu–ZrO$_2$(20) samples. Signals marked by asterisk correspond to Cu dimer species.
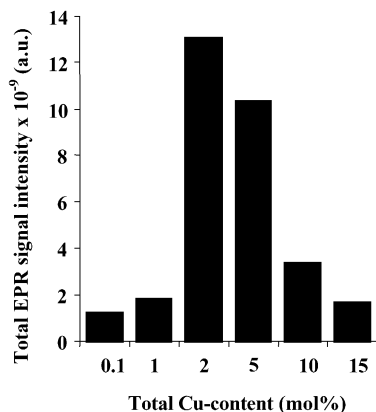
Fig. 4. Total EPR signal intensity as a function of Cu content in Cu–ZrO$_2$ samples.

Cu–ZrO$_2$(5) and species II, III and IV in Cu–ZrO$_2$(20) samples. The EPR spectra of Cu–ZrO$_2$(5) and Cu–ZrO$_2$(20) at different preheating temperatures are shown in Fig. 5. The spectrum of Cu–ZrO$_2$(5) preheated at 973 K corresponds mostly to species I only; the species II and III are absent perhaps due to the reduction of Cu^{2+} to Cu$^+$ on evacuation and removal of adsorbed water molecules. Similar observations were also noted in Cu–ZrO$_2$(20) sample, evacuated at higher temperatures. Species I was observed throughout the temperature range, while species II, III and IV decreased and finally disappeared at higher temperatures (Fig. 5). An additional weak signal (marked by asterisk) due to Cu dimers appeared at 1600 G. This signal was more predominant in Cu–ZrO$_2$(20) sample than in Cu–ZrO$_2$(5). At still higher temperatures (>973 K), a broad featureless signal was observed.

The influence of reaction with dry hydrogen is presented in Fig. 6. Cu–ZrO$_2$ samples with 0.1 and 5 mol % Cu were evacuated and reacted with dry hydrogen at 530 K. In addition to the signals due to species I, Cu–ZrO$_2$(0.1) showed signals at 2.002, 1.978 and 1.954. The former at 2.002 is attributed to O$^-$ species. The assignment of the latter signals is inconclusive. They were attributed in the past to electrons trapped in anion vacancies and also to Zr^{3+} ions [44,45]. Incorporation of Cu^{2+} ions in the framework of zirconia is probably the cause for the formation of these defect centers, which are responsible for the oxygen storage capacity (OSC) of these materials, an important property in fuel cell applications. Upon evacuation at 530 K, the intensity of signals due to the defects increased (Fig. 6 curve b). This could be due to the reduction of some amount of Cu from +2 to +1/0 valent state. The extent of reduction of Cu^{2+} was more and the intensity of O$^-$ signals increased by about 15 times when Cu–ZrO$_2$(0.1) sample was reacted with hydrogen. On the other hand, Cu–ZrO$_2$(5) sample showed signals due to Cu species I, II and III and O$^-$ ions. Upon reaction with hydrogen, species II and III disappeared (Fig. 6, curve c of the right panel). The spectrum contained signals due to species I only. The intensity of O$^-$-ion signal increased by two orders of magnitude. Thus, these studies reveal that among the different types of Cu, species I is relatively more difficult to reduce than species II, III and IV. This is apparent from the presence of signals due to species I even at 923 K.

Based on the EPR study, we infer the presence of four types of paramagnetic Cu species in Cu–ZrO$_2$(n) samples prepared by the sol–gel technique. A summary of the EPR parameters of these species in samples with increasing Cu content in zirconia is given in Table 3. Species I and II are present in all the Cu compositions. Species III is identified only in the samples containing 5 mol % or more of Cu, while species IV is present in samples containing 20 mol % or more of Cu in zirconia. Quantification of the individual species was not attempted as no reasonable estimate could
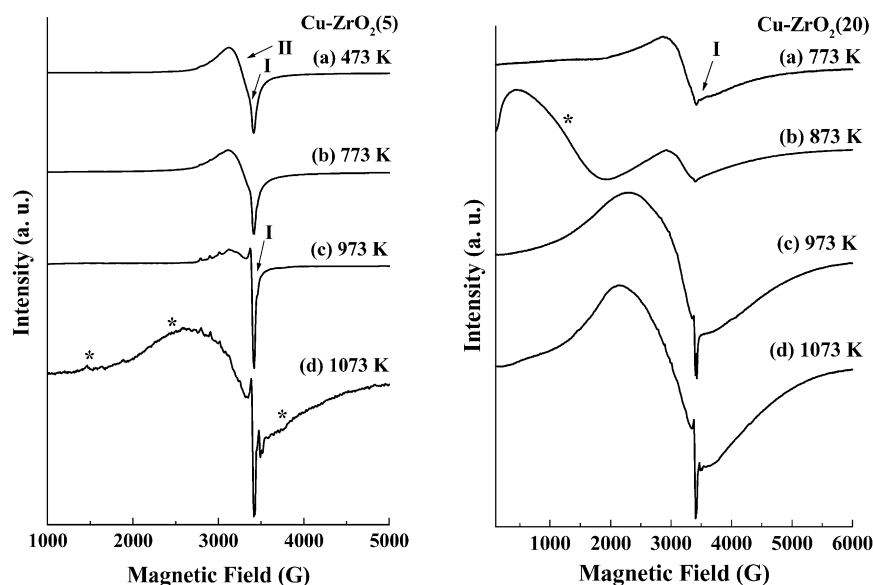

Fig. 5. Effect of preheating and evacuation on the EPR spectra of Cu–ZrO$_2$(5) and Cu–ZrO$_2$(20) samples.
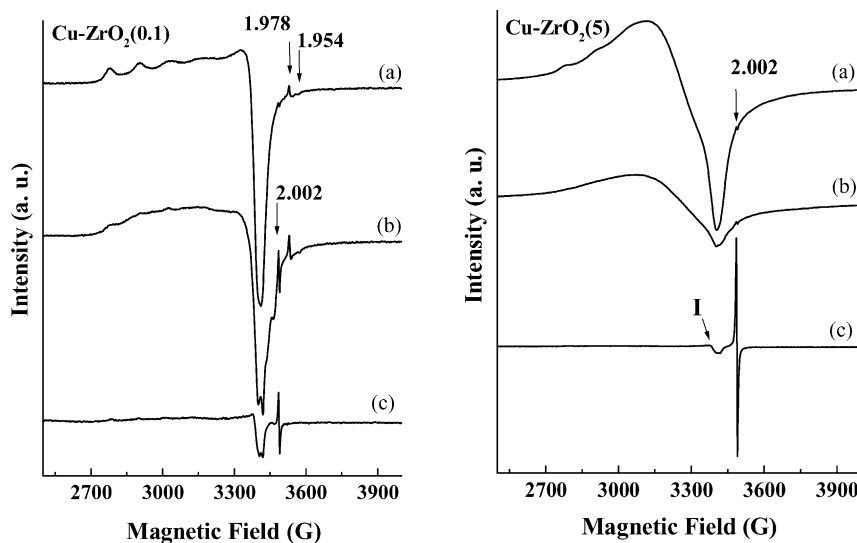
Fig. 6. Effect of thermal evacuation and hydrogen treatment on the EPR spectra of Cu–ZrO$_2$(0.1) and Cu–ZrO$_2$(5) samples. (a) After evacuation at 298 K; (b) after evacuation at 530 K and (c) after evacuation and reaction with hydrogen at 530 K.

be made from the complicated spectra of the present type. Species I and III exhibited resolved Cu hyperfine features indicating that these species correspond to well-dispersed Cu(II) ions. The rhombic g values ($g_x = 2.05$, $g_y = 2.08$ and $g_z = 2.35$) and a low $A_{\parallel}^{Cu}$ value (123.7 G) of species I indicate that these ions are in the framework substitutional positions and possess a low symmetry octahedral environment around Cu. The assignment of species I in framework locations reinforces the conclusions drawn from the XRD studies. The charge imbalance created by Cu substitution in the lattice is compensated by either creating defects in the lattice (oxide ion vacancies) or incorporating Cu^{2+} in interstitial positions. We presume that species II corresponds to dispersed interstitial Cu ions, as they exhibit isotropic signal and possess a perfect O$_h$ symmetry around them. Species III, characterized by an axial spectrum corresponds to tetragonally elongated square pyramidal type of Cu ions, which are bound to the external surface through hydroxyl groups of zirconia or located in the surface defect sites. Such species has already been characterized by EPR spectroscopy in zirconia samples impregnated with small concentrations of Cu ions [21]. The surface Cu sites are dispersed up to 20 mol % due to the high surface area of zirconia. Such a high dispersity was reported

also for chromia–zirconia catalysts [46]. Beyond 20 mol % Cu, interacting CuO-type clusters are formed (species IV). These species behave differently towards pre-heating. While the extra-lattice Cu (species II, III and IV) reduces on thermal treatment or reaction with hydrogen at 530 K, the framework Cu ions (species I) are stable even at 973 K.

The d–d band at 800 nm in the DRUV–Vis arises, therefore, from species I and II types of Cu^{2+} ions. The band at 660 nm (in 10 wt.% and above Cu compositons) is due to species III. The band at 380 nm is due to the 2–3 atom Cu nanoclusters. All these are dispersed Cu species. CuO-like phase (species IV), prevalent more in the samples containing ≥20 mol % Cu also shows the band at 380 nm.

Cu–ZrO$_2$ with 20 mol % Cu was found to be the most active sample in the oxidation of CH$_4$ and CO [27]. The structural and spectral studies reveal that Cu species is dispersed (in the form of isolated ions or 2–3 atom nanoclusters) up to 20 mol % concentration in zirconia and beyond that a CuO-type phase is formed. Although no quantification could be made, it appears that the amount of dispersed Cu species is more in Cu–ZrO$_2$(20) sample than in the other compositions. This high dispersion of Cu species, their facile redox behavior and the oxygen storage capability

Table 3
EPR g-values of Cu^{2+} species in Cu–ZrO$_2$(n) samples

Cu content mol % (n)	Signal I			Signal II	Signal III		Signal IV
	g_x	g_y	g_z	g_{av}	$g_\perp$	$g_\parallel$	g_{iso}
1	2.050	2.080	2.350	2.110	–	–	–
2	2.055	2.075	2.360	2.135	–	–	–
5	2.060	2.080	2.370	2.130	2.080	2.32	–
10	2.060	2.080	2.037	2.130	2.08	2.32	–
20	2.055	2.080	2.036	2.135			2.18
25	2.060	2.080	2.036	2.140	–	–	2.25
33	2.055	2.080	2.034	2.130	–	–	2.25

are the possible causes for the superior activity of Cu–$ZrO_2(20)$ samples in CH_4 and CO oxidations.

4. Conclusions

Some of the earlier studies on the phase transitions of zirconia as a result of incorporation of different metal oxides have been restricted by the observed XRD profiles. We have shown through the Rietveld refinement of the powder XRD profiles of Cu–$ZrO_2(n)$ samples that zirconia is not stabilized in cubic phase alone. For the samples prepared by co-precipitation or sol–gel techniques and calcined at 773 K, Cu–$ZrO_2(n)$ exists both in cubic and tetragonal phases. The relative amount of cubic phase increases with the increasing Cu content, at the expense of tetragonal phase. There appears to be an equilibrium between the two phases, which depends on the temperature of calcination, Cu content and the crystallite size. A higher concentration of Cu and smaller crystallite size, (based on the preparation technique) tend to stabilize zirconia in the cubic phase.

As far as the local environment and the location of Cu in zirconia are concerned, four types of paramagnetic Cu species, *viz.*, isolated, substitutional ions (species I), extra-lattice/interstitial ions (species II), dispersed surface bound ions (species III) and CuO clusters (species IV) have been identified by EPR spectroscopy and spectral simulations, depending on the concentration of Cu in zirconia. The first types of species are reported for the first time. Earlier reports on the Cu–ZrO_2 samples, prepared by impregnation method contained only the species type III and IV. These species behave differently towards pre-heating and reduction with hydrogen. As expected, the extralattice species (II, III and IV) reduce more easily than the framework-substituted Cu ions (species I). The structural (XRD) and spectral (EPR and DRUV–Vis) results are in agreement with the possible substitution of some Zr^{4+} by Cu^{2+} ions in the lattice. By either method of preparation, up to 20 mol %, Cu could be dispersed at the surface without forming CuO-type phase. The dispersed Cu species (II and III) are responsible for the catalytic activity of Cu–ZrO_2 in the oxidation of CH_4 and CO reported earlier.

Acknowledgement

References

[1] R. Stevens, An Introduction to Zirconia, second ed., Magnesium Electron Ltd., 1986.

[2] T. Yamaguchi, Catal. Today 20 (1994) 199.

[3] K. Arata, Adv. Catal. 37 (1990) 165.

[4] S.K. Saha, P. Pramanik, Bull. Ceram. Trans. 94 (1995) 123.

[5] C.F. Grain, J. Am. Ceram. Soc. 50 (1967) 288.

[6] R.P. Ingel, D. Lewis III, J. Am. Ceram. Soc. 69 (1986) 325.

[7] H. Ishizawa, O. Sakurai, N. Mizutani, M. Kato, Am. Ceram. Soc. Bull. 65 (1986) 1399.

[8] A.M. George, N.C. Mishra, N.C. Jayadevan, J. Mater. Sci. Lett. 11 (1992) 404.

[9] R.-X. Zhou, X.-Y. Jiang, J.-X. Mao, X.-M. Zheng, Appl. Catal. A Gen. 162 (1997) 213.

[10] T.H. Etsell, S.N. Flengas, Chem. Rev. 70 (1970) 339.

[11] A. Keshavaraja, A.V. Ramaswamy, J. Mater. Res. 9 (1994) 837.

[12] M. Hoch, M. Mathur, J. Am. Ceram. Soc. 45 (1962) 373.

[13] J.C. Ray, P. Pramanik, S. Ram, Mater. Lett. 48 (2001) 281.

[14] V. Indovina, Catal. Today 41 (1998) 95.

[15] K.A. Bethke, M.C. Kung, B. Yang, M. Shah, D. Alt, C. Li, H.H. Kung, Catal. Today 26 (1995) 169.

[16] D. Pietrogiacomi, D. Sannino, A. Magliano, P. Ciambelli, S. Tuti, V. Indovina, Appl. Catal. B Environ. 36 (2002) 217.

[17] K. Tanabe, T. Yamaguchi, Catal. Today 20 (1994) 185.

[18] Y.-W. Suh, S.-H. Moon, H.-K. Rhee, Catal. Today 63 (2000) 447.

[19] K.-D. Jung, A.T. Bell, J. Catal. 193 (2000) 207.

[20] A.T. Bell, Stud. Surf. Sci. Catal. 136 (2001) 13.

[21] J. Liu, J. Shi, D. He, Q. Zhang, X. Wu, Y. Liang, Q. Zhu, Appl. Catal. A Gen. 218 (2001) 113.

[22] C. Morterra, E. Giamello, G. Cerrato, G. Centi, S. Perathoner, J. Catal. 179 (1998) 111.

[23] N. Kiratzis, Fuel Cells 1 (2001) 211.

[24] R.J. Gorte, H. Kim, J.M. Vohs, Preprints, ACS Div. Fuel Chem. 46 (2001) 678.

[25] S. Velu, K. Suzuki, M. Okazaki, M.P. Kapoor, T.O. Saki, F. Ohashi, J. Catal. 194 (2000) 373.

[26] S. Park, R.J. Gorte, J.M. Vohs, Appl. Catal. A Gen. 200 (2000) 55.

[27] M.K. Dongare, V. Ramaswamy, C.S. Gopinath, A.V. Ramaswamy, S. Scheurell, M. Bruechner, E. Kemnitz, J. Catal. 199 (2001) 209.

[28] O.V. Metelkina, V.V. Lunin, V.A. Sadykov, G.M. Alikina, R.V. Bunina, E.A. Paukshtis, V.B. Fenelonov, A.Yu. Derevyankin, V.I. Zaikovski, U. Schubart, J.R.W. Ross, Catal. Lett. 78 (2002) 111.

[29] R.C. Garvie, J. Phys. Chem. 69 (1965) 1238;
R.C. Garvie, J. Phys. Chem. 82 (1978) 218.

[30] V.S. Stubican, J.R. Hellman, in: Advanced Ceramics III, Science and Technology of Zirconia, 1981, p. 25.

[31] M. Yashima, S. Sasuki, M. Kakihana, Y. Yamaguchi, H. Arashi, M. Yoshimura, Acta. Cryst. B 14 (1995) 381.

[32] A. Clearfield, J. Mater. Res. 5 (1990) 161.

[33] L.E. Depero, P. Levrangi, J. Solid State Chem. 110 (1994) 190.

[34] G. Pang, S. Chen, Y. Zhu, O. Palchik, Y. Koltypin, A. Zaban, A. Gedanken, J. Phys. Chem. B 105 (2001) 4647.

[35] F. Tietz, W. Jungen, P. Lersch, Chem. Mater. 14 (2002) 2252.

[36] D.G. Lamas, N.E. Walsue De Reca, J. Mater. Sci. 35 (2000) 5563.

[37] G.E. Lascalea, D.G. Lamas, E. Djurado, N.E. Walsue De Reca, in: Proceedings of 22nd International Symposium Materials Science, Denmark, 2001, p. 313.

[38] J.A. Wang, M.A. Valenzuela, J. Salmones, A. Vázquez, A. García-Ruiz, X. Bokhimi, Catal. Today 68 (2001) 21.

[39] M. Bhagwat, A.V. Ramaswamy, A.K. Tyagi, V. Ramaswamy, Mater. Res. Bull. 38 (2003) 1713.

[40] D.G. Lamas, N.E. Walsue De Reca, Mater. Lett. 41 (1999) 204.

[41] H.P. Klug, L.E. Alexander, X-ray Diffraction Procedures: For Polycrystalline and Amorphous Materials, John Wiley and Sons, New York, 1974, p. 618.

[42] Y. Wang, R.C. Caruso, J. Mater. Chem. 12 (2002) 1442.

[43] Z. Liu, W. Ji, L. Pong, Y. Chen, J. Catal. 172 (1997) 243.

[44] A. Martínez-Arias, M. Fernández-García, L.N. Salamanca, R.X. Valenzuela, J.C. Conesa, J. Soria, J. Phys. Chem. B 104 (2000) 4038.

[45] A. Martínez-Arias, M. Fernández-García, V. Ballesteros, L.N. Salamanca, J.C. Conesa, C. Otero, J. Soria, Langmuir 15 (1999) 4796.

[46] D. Cimino, D. Cordischi, S. De Rossi, G. Ferraris, D. Gazzoli, V. Indovina, G. Minelli, M. Occhiuzzi, M. Valigi, J. Catal. 127 (1991) 744.